Ion Mobility of Ground and Excited States of Laser-Generated Transition Metal Cations

Yehia Ibrahim, Edreese Alsharaeh, Ridha Mabrouki, Paul Momoh, Enli Xie, and M. Samy El-Shall*

Department of Chemistry, Virginia Commonwealth University, Richmond, Virginia 23284-2006

Received: September 17, 2007; In Final Form: October 8, 2007

The application of ion mobility to separate the electronic states of first-, second-, and third-row transition metal cations generated by the laser vaporization/ionization (LVI) technique is presented. The mobility measurements for most of the laser-generated transition metal cations reveal the presence of two or three mobility peaks that correspond to ground and excited states of different electronic configurations. The similarity of the measured reduced mobilities for the metal cations generated by LVI, electron impact, and glow discharge ion sources indicates that the same electronic configurations are produced regardless of the ion source. However, in comparison with electron impact of volatile organometallic compounds, the LVI populates fewer excited states due to the thermal nature of the process. Significant contributions to the production and populations of excited states of Ni^+, Nb^+, and Pt^+ cations have been observed in the presence of argon during the LVI process and attributed to the Penning ionization mechanism. The origin of the mobility difference between the ground and the excited states is mainly due to the different interaction with helium. The ratio of the reduced mobilities of the excited and ground states decreases as one goes from the first- to the second- to the third-row transition metal cations. This trend is attributed to the ion size, which increases in the order $6sd^{n-1} > 5sd^{n-1} > 4sd^{n-1}$. This work helps to understand the mechanisms by which transition metal cations react in the gas phase by identifying the ground and excited states that can be responsible for their reactivity.

I. Introduction

Pulsed laser vaporization is a well-established powerful technique to generate a variety of gas-phase metal atoms, ions, neutral clusters, cluster ions, and nanoparticles for a wide range of studies and applications ranging from gas-phase reactions, ion thermochemistry, spectroscopy, and dynamics of clusters to nanostructured materials, thin films, and multilayers.[1−5] A high-power laser pulse focused on a metal target can create, within the duration of the pulse, instantaneous surface temperatures well above the boiling point of any metal. The generated plasma can vaporize and ionize the ejected species from any material, regardless of its boiling point, thus producing both atoms and ions. For example, laser vaporization/ionization (LVI) of metals using nanosecond lasers typically generates a large number of metal atoms ($\sim 10^{14}$), a small fraction of singly charged atomic ions ($\sim 10^6$), and a much smaller fraction of multiply charged ions.[1−4] Other species that are normally generated include fast electrons accelerated by the absorption of laser radiation. Generation of the metal ions is viewed as a combination of thermal, plasma, and multiphoton ionizations. In addition, electron impact (EI) via collisions of fast electrons with metal atoms is considered to play a major role in the ion production, particularly under confined plasma conditions.[1−3]

Laser-generated ions have been used extensively in many chemistry and physics investigations, particularly those involving mass spectrometric techniques such as ion cyclotron resonance (ICR), time-of-flight (TOF), guided ion beam, and high-pressure mass spectrometry to study ion−molecule reaction kinetics, binding energies, spectroscopy, and structure.[6−14] The contributions of the metal ion excited states to the ion−molecule chemistry of the laser-generated ions can be very significant. These contributions depend on the nature and lifetime of the excited state, the time scales of the specific measurements, and

the experimental conditions associated with the LVI. For example, the excited-state contributions may not be significant in experiments involving relatively long time scales and large numbers of ion−gas collisions where the excited-state species can be relaxed. However, in other experiments involving short time scales and low pressures, the excited reactant species can create major problems. In this case, the observation of endothermic reactions in metal ion−molecule reactions is often considered as an indication of the presence of excited states of the metal ions generated by LVI. Clearly, the exact contributions of excited states to the observed chemistry are difficult to understand if the electronic-state distributions of the reactant ions under the reaction conditions are not directly determined.

Transition metal (TM) ions are characterized by a large number of low-lying electronic states that can be easily accessed under the typical LVI conditions.[14] Because most of the low-lying electronic states of first-row TM cations have either a $3d^n$ or a $4s^1 3d^{n-1}$ electronic configuration, most of the transitions between these states are parity forbidden. Therefore, the radiative life times of the excited states can be on the order of milliseconds or even seconds, which allow the experimental observation of these states.[15] The chemistry of such metal ions is very much dependent on the type of states present.[16] Thus knowing the population of these different electronic states is essential to unlock the complex chemistry of TM ions. Several studies have applied the ion mobility technique to separate and characterize the electronic states of TM ions produced by EI and glow discharge (GD).[17−22] These studies were pioneered by Bowers and co-workers who introduced the term "electronic-state chromatography" after demonstrating the ability of helium gas to separate the electronic configurations of transition metal ions in ion mobility experiments.[17−19,24−26] They studied the electronic states of first-row TM ions produced by EI of volatile

Ion Mobility of Laser-Generated Cations

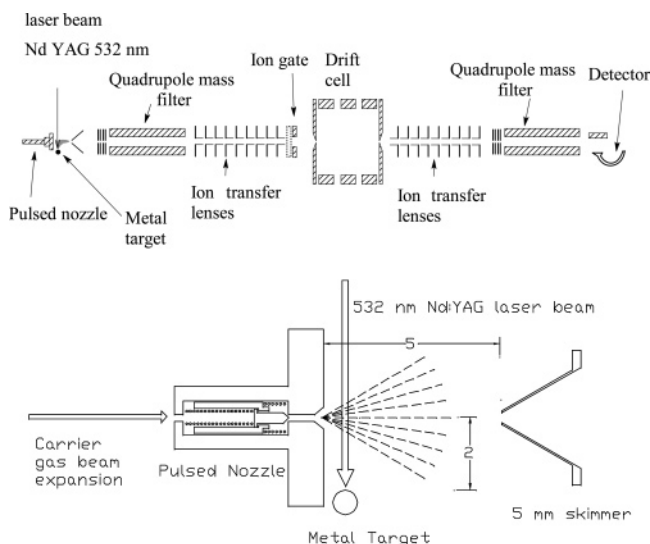*J. Phys. Chem. A, Vol. 112, No. 6, 2008* **1113**

Figure 1. Schematic diagram of the mass-selected ion mobility system coupled to the laser vaporization/ionization (LVI) source.

organometallic compounds. The separation of the electronic states is based on the interaction with helium. TM ions with electronic states that have repulsive interactions with helium, such as those with the $4s^1 3d^{n-1}$ configuration, move faster and thus have higher mobilities. The repulsive interaction of the 4s orbital on the metal with the filled $1s^2$ orbital of helium prevents capture collisions from occurring with the helium buffer gas, and these ions proceed rapidly through the mobility cell.

Recently, we reported the first application of ion mobility to characterize the electronic configurations of TM ions generated by LVI and to provide evidence for the significant contribution of Penning ionization to the production of excited-state ions in the LVI processes.[27] These studies can provide critical information on the nature of the electronic states accessible within different LVI experiments (for example, by using IR, visible, or UV lasers under different power density regimes) and on the relative populations of excited states of ions generated by different ionization methods. Furthermore, it would be possible to reveal the different mechanisms by which excited metal ion states might be produced in the LVI experiments. These studies can also help in developing new approaches to study state-selected ion−molecule reactions. In this paper, we present a comprehensive study of the electronic-state ion mobilities of the metal cations V^+, Cr^+, Fe^+, Ni^+, Cu^+, Zr^+, Nb^+, Pd^+, Ag^+, Cd^+, Pt^+, and Au^+ generated by the LVI technique. We also compare the electronic-state populations of the laser-generated metal ions with those generated by electron impact and glow discharge ion sources.[17−21] The ground- and excited-state mobilities of Zr^+, Nb^+, and Cd^+ are reported here for the first time. The experimental parameters that influence the observation of excited states and their relative populations are presented and discussed.

II. Experimental Section

Our mass-selected ion drift cell apparatus has been described previously.[27−29] The experimental setup for the LVI source coupled to the ion mobility system is displayed in Figure 1. The essential parts of the apparatus are jet and beam chambers coupled to a quadrupole mass filter, a drift tube, and a second quadrupole mass spectrometer. The metal cations are generated by pulsed LVI using the second harmonics of a Nd:YAG laser (532 nm, 2−30 mJ/pulse operated at 30 Hz) of a selected rotating and translating metal target.

The hot ions travel about 20 mm before overlapping with a pulse of Ar atoms and clusters formed by expanding 6 atm of Ar gas through a pulsed nozzle (General Valve series 9) of a 0.5 mm conical orifice. The ions are then swept toward a 5 mm skimmer (coaxial with the nozzle) by the effect of the Ar expansion. The ion beam passes into the second chamber, which is typically maintained at 2×10^{-6} Torr. The metal cations are mass-selected using the quadrupole mass filter, and the selected ions are focused into the drift cell for the mobility measurements as described below. Because the measured mobilities of the mass-selected ions were found to be the same as those with the first quadrupole operating in radio frequency (RF) only mode, most of the measurements were performed under RF only mode to maximize the ion signal. No metal cluster ions are produced in the current LVI setup because the generated metal atoms are not confined nor expanded through the nozzle. The ion pulse is gated using an ion gate and injected into a drift cell filled with about 2.5 Torr of He. Cell entrance and exit holes are 0.5 mm, and the drift cell length is 9 cm. A weak uniform electric field is applied to drift the ions from the cell entrance to the exit. Upon exiting the cell, the ions are collected and refocused to the second quadrupole for analysis and detection. The second quadrupole mass filter is used to monitor the arrival time distribution (ATD) of a particular m/z ion or to obtain a mass scan of the exiting ions. The ions are detected by an off-axial conversion dynode-electron multiplier detector. A pulse/delay generator is used to synchronize the timings between the laser, nozzle, ion gate, and data acquisition. The ion pulse from the source has a typical width of 5−10 μs. The ion-gate pulse triggers a multichannel scalar (2 μs/channel resolution), and the ion intensity is collected as a function of time, giving the ATD of a particular m/z ion.

Mobility Measurements. The ATD is collected at different P/V values (P is the cell pressure in Torr, and V the drift voltage in V). Plotting the ATD of a specific mobility peak (taken at the peak maximum, assuming Gaussian distribution) versus P/V gives a linear plot with a slope inversely proportional to the ion reduced mobility (K_0)[30] where

$$K = \frac{\vec{v}_d}{\vec{E}} = \frac{z/t_d}{V/z} \tag{1}$$

$$K_0 = K \frac{P}{760} \frac{273.15}{T} \tag{2}$$

$$t_d = \left(\frac{z^2 \times 273.15}{760 T K_0}\right)\frac{P}{V} + t_0 \tag{3}$$

Here, $\vec{v}_d$ is the ion drift velocity, $\vec{E}$ is the drift field, z is the drift length, t_d is the peak arrival time (peak center), K is the mobility, T is the temperature in Kelvin, and t_0 is the time ions spent outside the cell. The above procedure assumes that the cell length is the ion drift length; i.e., the ions do not penetrate inside the cell. (The ions are thermalized at the cell entrance.) We tested this assumption by measuring the mobility at different relative injection energies, and the measured mobilities did not differ by more than 4% in the worst case. The mobilities reported here are measured with the lowest possible injection energies required to introduce the ions into the cell against the helium flow. These energies depend on the laser powers used in the LVI process, which determine the kinetic energies of the generated ions. Finally, the mobilities are measured in the low-field limit where the ion's drift velocity is small compared to the thermal velocity and the ion mobility is independent of the field strength (E/N < 6.0, where E is the electric field intensity

TABLE 1: Summary of the Measured Reduced Mobilities for the Transition Metal Cations. The Total Uncertainty in the Measured Mobility Is 3%

| | | Population % | | | K_0 (cm^{2}V^{-1}s^{-1}) | | | |
| | | | EI[18,19] | | | | | |
ion	peak	this work	30 eV	T (K)	this work	ref 18 ($\pm$7%)	ref 20	ref 23
V$^+$	I	1−7	25	300	25.3	25.1		
	II	14−34	25		21.8	22.0	21.4 $\pm$ 0.2	
	III	85−59	50		16.4	16.7	16 $\pm$ 1	
Cr$^+$	I	28−52	13	300	22.8	21.4		24.6 $\pm$ 2.5
						20.4		
	II	72−48	86		18.3	17.5	18.0 $\pm$ 0.3	18.9 $\pm$ 1.9
Fe$^+$	I		92	302	23.5	23.7	23 $\pm$ 1	
						16.9		
Ni$^+$	I	36−12	84	305	24.1	24.2	24 $\pm$ 2	
	II	64−87	16		16.3	16.3	16.2 $\pm$ 0.2	
Cu$^+$	I	10−16		297	24.1		22 $\pm$ 1	
	II	90−84	100		16.1	15.7	15.8 $\pm$ 0.6	
Zr$^+$	I	99.8		299	25.3			
	II	0.2			17.2			
Nb$^+$	I	26−45		299	19.7			
	II	74−55			15.5			
Mo$^+$	I	100		299	20.6			23.4 $\pm$ 2.3
								18.5 $\pm$ 1.9
Pd$^+$	I	8−2		303	22.9		23.2 $\pm$ 0.4	
	II	92−98			18.1		18.2 $\pm$ 0.6	
Ag$^+$	I	22−43		299	22.1			
	II	78−66			17.7		18 $\pm$ 1	
Cd$^+$	I	100		299	22.2			
Pt$^+$	I	20		302	20.8		23 $\pm$ 2	
	II	80			18.3		20.6 $\pm$ 0.9	
Au$^+$	I	30		303	20.4		22 $\pm$ 2	
	II	70			18.1		19.5 $\pm$ 0.5	

and N is the gas number density and E/N is expressed in units of Townsend (TD) where 1 TD = 10^{-17} V cm^2).[30]

The measured ATD can be calculated from the transport theory for a short packet (delta pulse) of ions injected into a cylindrical drift tube through an aperture of area a using eq 4[30,31]

$$\phi(t) = \frac{sa\, e^{-\alpha_t}}{4\sqrt{\pi D_L t}}\left(v_d + \frac{l}{t}\right)\left(1 - \exp\left(-\frac{r_0^{\,2}}{4D_T t}\right)\right)$$
$$\exp\left(-\frac{(l - v_d t)^2}{4D_L t}\right) \quad (4)$$

The ions are introduced as a delta pulse in the form of an axially thin disk of radius r_0 and uniform surface density s. The term s is used as a scaling factor for the signal intensity. Loss of ions through reactions during the drift time can be accounted for through the frequency factor α. D_L and D_T are the longitudinal and transverse diffusion coefficients. Under low-field conditions the ion diffusion coefficients D_L and D_T are related to the mobility by the Einstein equation[30]

$$D_L = D_T = K\frac{k_B T}{ze} \quad (5)$$

where ze is the number of charges times the charge of the electron and k_B is Boltzmann's constant.

III. Results and Discussion

In this work, we measured the mobilities of the laser-generated atomic cations of vanadium, chromium, iron, nickel, copper, zirconium, niobium, molybdenum, palladium, silver, cadmium, platinum, and gold. The results are summarized in Table 1 while Tables 2 and 3 provide the assignments and energetics of the low-lying electronic states[32] of the metal ions

investigated in this work. In section A, we present and discuss the mobility results for each of the metal cations studied and compare the results with those obtained using different ion sources. In section B, we discuss the effects of different experimental parameters such as the expansion carrier gas, the laser power, and buffer gas pressure and temperature.

A. Electronic-State Ion Mobilities. *1. Vanadium.* Figure 2a displays a typical mass spectrum obtained following the injection of V$^+$ into the drift tube containing 2.0 Torr He. The mass spectrum of V$^+$ shows mainly the 51 m/z ion, which is the most abundant isotope of vanadium. The ATDs of ^{51}V$^+$ show three peaks labeled I, II, and III as shown in Figure 2a. To assign the ground and excited electronic states we varied the laser power as shown in Figure 2b and in the inset of Figure 2b. The laser power study indicates that the ground electronic state is included in peak III because its population decreased with increasing laser power while the excited states are included in peaks I and II. Peaks III, II, and I were assigned previously as ground, first excited, and higher excited electronic states of V$^+$ produced by EI ionization of VOCl$_3$.[18] The ground electronic state of V$^+$ is a (^{5}D) 3d^4 state while the excited states that are closely spaced are either 4s^{1}3d^3 or 3d^4 states of triplet or pentet multiplicity (Table 2).[32] Peak II was assigned by Kemper and Bowers to the (^{5}F) 4s^{1}d^3 and (^{3}F) 4s^{1}d^3 states, while peak I was assigned to high-energy states (>2.4 eV) of the 4s^{1}d^3 configuration.[15,33] The population of the ground state (peak III) for V$^+$ produced by LVI is higher than that produced by electron impact (75% in this work versus 50% for the 30 eV EI).[18] This is an indication of the different ion generation mechanism in the LVI process, which produces metal ions by ionizing the ground-state metal atoms, while in EI the ions are produced from already excited atoms following the decomposition of the precursor molecules. The mobilities of the three peaks were measured by collecting the ATDs of ^{51}V$^+$ at different drift fields and plotting the ATD versus P/V for each peak as shown in Figure 2c. The reduced

Ion Mobility of Laser-Generated Cations

J. Phys. Chem. A, Vol. 112, No. 6, 2008 **1115**

TABLE 2: Low-Lying Electronic States for the First-Row Transition Metal Cations[a]

ion	state	configuration	energy (eV)	ion	state	configuration	energy (eV)
V$^+$	**^{5}D**	**3d^4**	**0.026**	Cr$^+$	**^{6}S**	**3d^5**	**0.000**
	^{5}F	4s3d^3	0.363		^{6}D	4s3d^4	1.522
	^{3}F	4s3d^3	1.104		^{4}D	4s3d^4	2.458
	^{3}P	3d^4	1.452		^{4}G	3d^5	2.544
	^{3}H	3d^4	1.566		^{4}P	3d^5	2.406
	^{3}F	3d^4	1.681		^{4}D	3d^5	3.104
	^{5}P	4s^{3}d^3	1.692				
	^{3}G	3d^4	1.807				
Ni$^+$	**^{2}D**	**3d^9**	**0.075**	Fe$^+$	**^{6}D**	**4s^{3}d^6**	**0.052**
	^{4}F	4s3d^8	1.160		^{4}F	3d^7	0.300
	^{2}F	4s3d^8	1.757		^{4}D	4s3d^6	1.032
	^{4}P	4s3d^8	2.899		^{4}P	3d^7	1.688
Cu+	**^{1}S**	**3d^{10}**	**0.000**		^{2}G	3d^7	1.993
	^{3}D	4sd^9	2.808		^{2}P	3d^7	2.299
	^{1}D	4sd^9	3.256				

[a] Ground states are in bold. Energy levels are statistically averaged over *J*-levels. Moore, C. E. *Atomic Energy Levels as Derived from the Analyses of Optical Spectra*; U. S. National Bureau of Standards, U. S. Government Printing Office: Washington, DC, 1971.

TABLE 3: Low-Lying Electronic States for the Second- and Third-Row Transition Metal Ions[a]

ion	state	configuration	energy (eV)	ion	state	configuration	energy (eV)
Zr$^+$	**^{4}F**	**5s4d^2**	**0.094**	Pd$^+$	**^{2}D**	**4d^9**	**0.176**
	^{4}F	4d^3	0.406		^{4}F	5s4d^8	3.369
	^{2}D	5s4d^2	0.546		^{2}F	5s4d^8	4.116
	^{2}P	5s4d^2	0.742		^{4}P	5s4d^8	4.589
	^{2}F	5s4d^2	0.764		^{2}D	5s4d^8	5.027
	^{4}P	5s4d^2	0.974				
	^{2}G	4d^3	0.993				
	^{4}P	4d^3	1.218				
	^{2}H	4d^3	1.511				
Nb$^+$	**^{5}D**	**4d^4**	**0.096**	Ag$^+$	**^{1}S**	**4d^{10}**	**0.000**
	^{5}F	5s4d^3	0.421		^{3}D	5s4d^9	5.034
	^{3}P	4d^4	0.833		^{1}D	5s4d^9	5.709
	^{3}F	5s4d^3	0.990				
	^{3}H	4d^4	1.225	Cd$^+$	**^{2}S**	**5s4d^{10}**	**0.000**
	^{3}G	4d^4	1.319		^{2}P	5p4d^{10}	5.677
	^{5}P	5s4d^3	1.368		^{2}D	5s^{2}4d^9	8.866
Mo$^+$	**^{6}S**	**4d^5**	**0.000**	Pt$^+$	**^{2}D**	**5d^9**	**0.418**
	^{6}D	5s4d^4	1.587		^{4}F	6s5d^8	1.177
	^{4}G	4d^5	1.906		^{4}P	6s5d^8	2.366
	^{6}P	4d^5	1.950		^{2}F	6s5d^8	2.529
	^{4}D	4d^5	2.120				
	^{2}D	4d^5	2.804	Au$^+$	**^{1}S**	**5d^{10}**	**0.000**
	^{2}I	4d^5	2.867		^{3}D	6s5d^9	2.288
	^{4}F	4d^5	2.964		^{1}D	6s5d^9	3.672

[a] Ground states are in bold. Energies are statistically averaged over *J*-levels. Moore, C. E. *Atomic Energy Levels as Derived from the Analyses of Optical Spectra*; U. S. National Bureau of Standards, U. S. Government Printing Office: Washington, DC, 1971.

mobilities for peaks I, II, and III are measured as 25.3, 21.8, and 16.4 cm^2 V^{-1} s^{-1}, respectively. The measured reduced mobilities are in excellent agreement with those reported by EI and GD ion sources as shown in Table 1,[18,20] thus indicating that the same electronic configurations are observed using different ionization sources. Also, the measured ATDs agree well with the predictions from transport theory (eq 4) for three independent species under the same experimental conditions as shown in Figure 2a. The small filling in ATDs between peaks I and II may be due to the relaxation of the electronic state of peak I to the electronic state of peak II. The electronic-state relaxation is believed to occur during the drift time through the cell where the ions experience many collisions with helium.

It should be noted that the assignments of the electronic states in the present work are based on the laser power studies of the observed ATD peaks that can distinguish between ground and higher-energy states of different configurations and also on assignments made by Kemper and Bowers in the EI experiments.[18] The differences between the ionization mechanisms in the EI and the present LVI experiments are expected to affect

mostly the relative populations of the different electronic states. The agreement between the measured mobilities in the present LVI results and the previous EI experiments indicate that states with the same electronic configurations are produced by both methods. However, the presence of different states with the same configurations can be tested using charge-transfer bracketing experiments as demonstrated by the work of Taylor et al.[20−22] The charge-transfer bracketing experiments involving metal cations generated by LVI and using appropriate charge-transfer molecules such as C$_3$H$_8$ and CH$_3$Br are currently under investigation in our laboratory, and the results will be published elsewhere.[34]

2. Chromium. The mass spectrum of the laser-generated chromium ions is displayed in Figure 3, which shows the ^{52}Cr ion. The ATDs of ^{52}Cr$^+$ are comprised of two peaks with populations strongly dependent on the laser power. The laser power study (inset of Figure 3) indicates that the ground state is included in peak II while excited states are included in peak I. The ground-state configuration (Table 2) of Cr$^+$ is (^{6}S) 3d^5 while the excited states are either (^{6}D or ^{4}D) 4s^{1}3d^4 or quartet
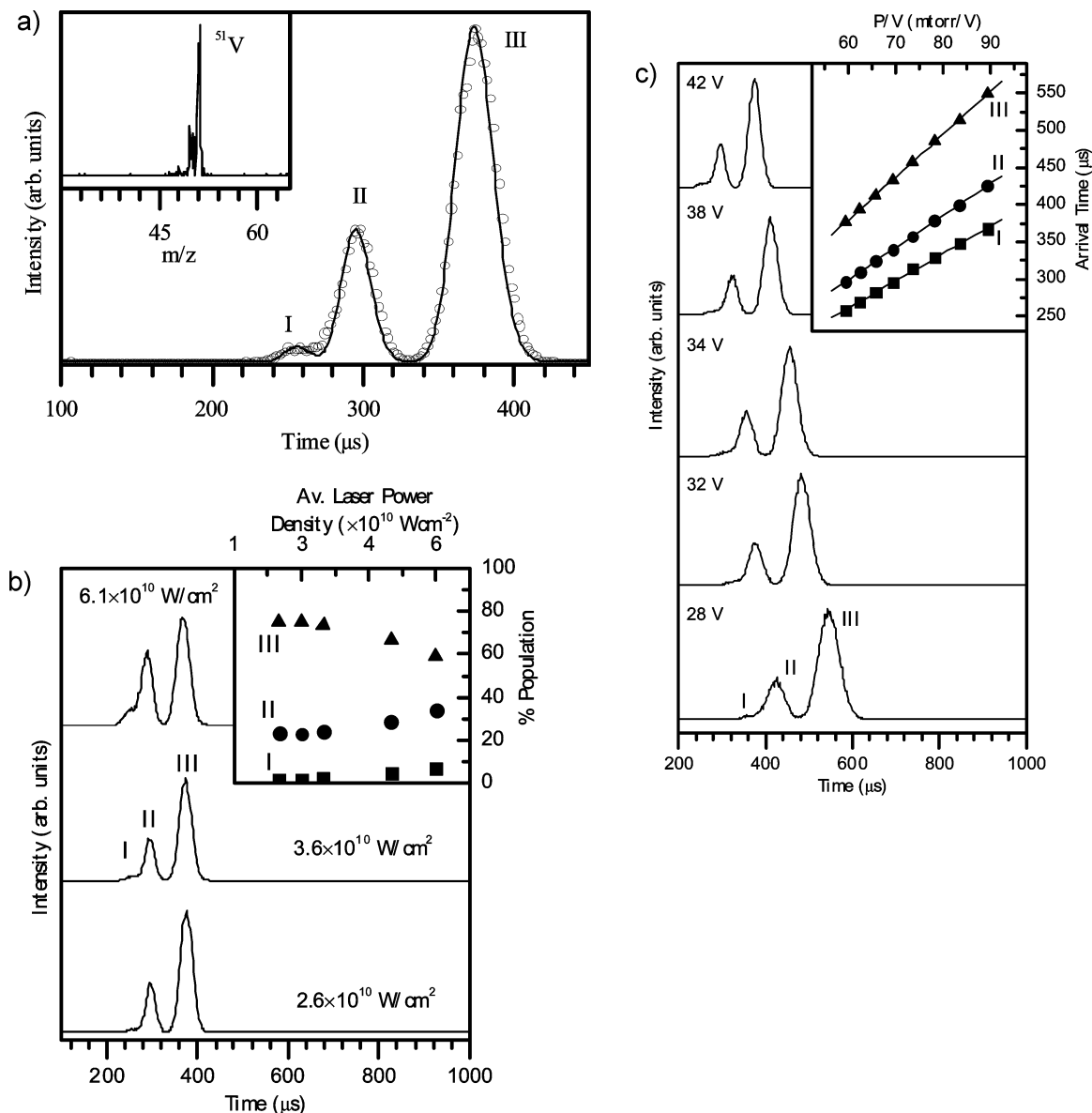
Figure 2. (a) Experimental ATDs of V^+ ions (circles) and the predicted distributions from transport theory (solid line). Inset shows the mass spectrum of V^+ ions. The apparent mass peak at m/z 50 is due to low signal intensity, which results in poor ion signal statistics. (b) ATDs of V^+ ions obtained at different laser powers. The inset shows the effect of laser power on the populations of the V^+ ion ground state III (triangles), first excited states II (circles), and second excited states I (squares). (c) ATDs of V^+ ions collected as a function of drift voltage. The inset shows plots of P/V vs arrival time for the V^+ ion electronic states included in peaks I, II, and III.

states with the $3d^5$ electronic configuration, and the transition from the excited state (^6D, $4s^13d^4$) to the ground state is parity forbidden.[31] The measured zero-field reduced mobilities are 18.3 and 22.8 cm^2 V^{-1} s^{-1} for the ground state (peak II) and excited state (peak I), respectively. These values match well with the K_0 values of the ground and the second excited states reported in the EI study of Kemper and Bowers.[18] However, the first excited state of Cr^+ reported in the EI study[18] is not observed in the current LVI study. The slight mismatch between the experimental ATDs and the predictions of transport theory in the region between the two peaks, shown in Figure 3, could be attributed to a third unresolved peak that could represent the first excited state observed in the EI study.

3. Iron. The mass spectrum of the laser-generated Fe^+ (inset in Figure 4) shows the natural isotopes of $^{54}Fe^+$ and $^{56}Fe^+$. The $^{57}Fe^+$ and $^{58}Fe^+$ isotopes are in low abundance (<2%) and are not resolved from the $^{56}Fe^+$ mass peak. The ATD of $^{56}Fe^+$ shows a tailing to longer times (Figure 4), which suggests either the presence of an unresolved electronic state or the incomplete

relaxation of a low-mobility state. The measured zero-field reduced mobility of the observed ATD peak is 23.5 cm^2 V^{-1} s^{-1}, which compares very well with the literature values of 23.7 and 23 cm^2 V^{-1} s^{-1}.[18,20] This peak is assigned to the (^6D) $4s^13d^6$ ground state and the (^4D) $4s^13d^6$ second excited state of Fe^+. However, a second low-mobility peak was observed in the EI study and assigned to higher-energy excited states with low populations (8% at 30 eV EI) and average reduced mobility of 16.9 cm^2 V^{-1} s^{-1}.[18] We attribute the tailing observed in the ATD of Fe^+ in our experiment (Figure 4) to collisional relaxation of these high-energy excited states during the drift time. This tailing was also observed by Taylor et al. in the glow discharge experiments of Fe^+.[20]

Kemper and Bowers assigned the low-mobility peak observed in the EI experiments to the (^4F) $3d^7$, (^4P) $3d^7$, and (^2G) $3d^7$ excited states.[18] This is consistent with the observation of the (^4F) $3d^7$ first excited state of Fe^+ with a population of ~10% in guided ion beam experiments using a laser vaporization source.[35] The binding energy of the (^4F) $3d^7$ excited state with

Ion Mobility of Laser-Generated Cations

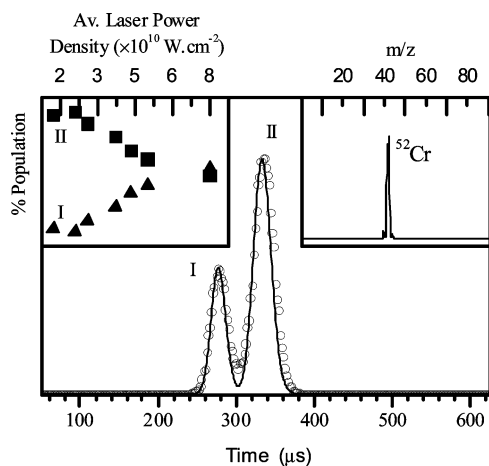*J. Phys. Chem. A, Vol. 112, No. 6, 2008* **1117**

Figure 3. Experimental ATDs of Cr$^+$ ions (circles) and the predicted distributions from transport theory (solid line). The insets show the mass spectrum of Cr$^+$ ions (right) and the effect of laser power on the populations of the Cr$^+$ ion ground state II (squares) and excited state I (triangles).
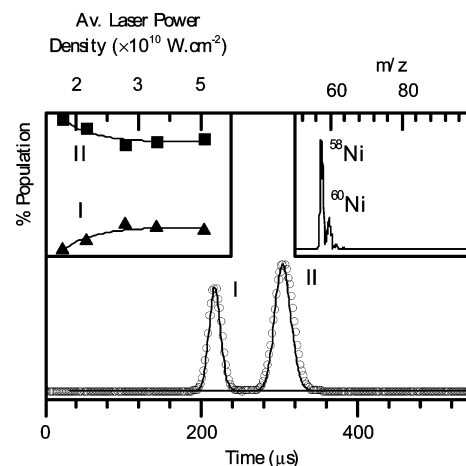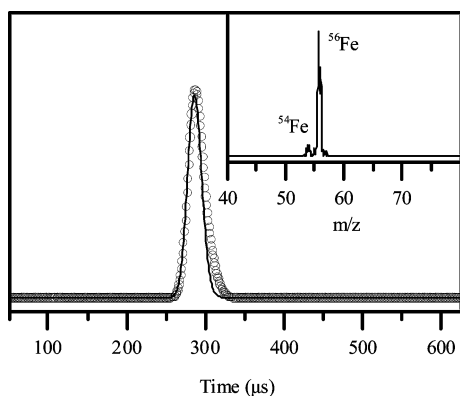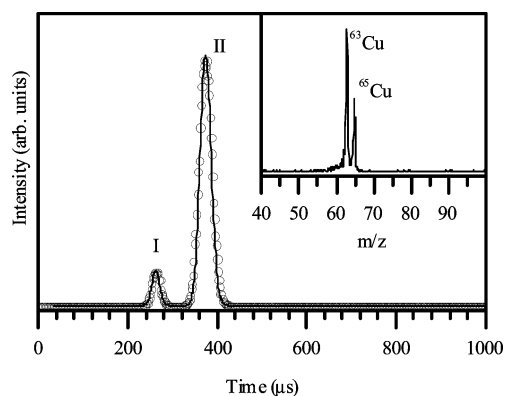

Figure 5. Experimental ATDs of Ni$^+$ ions (circles) and the predicted distributions from transport theory (solid line). The insets show the mass spectrum of Ni$^+$ ions (right) and the effect of laser power on the populations of the Ni$^+$ ion ground state II (squares) and excited state I (triangles).

Figure 4. Experimental ATDs of Fe$^+$ ions (circles) and the predicted distributions from transport theory (solid line). The inset shows the mass spectrum of Fe$^+$ ions.

Figure 6. Experimental ATDs of Cu$^+$ ions (circles) and the predicted distributions from transport theory (solid line). The inset shows the mass spectrum of Cu$^+$ ions.

He ($D_e = 0.144$ eV for the $^4\Sigma^-$ state)[36] is greater than that of the (^{6}D) $4s^13d^6$ ground state ($D_e = 0.014$ eV for the ^{6}D state),[36] which allows for curve crossing leading to an excited-state relaxation. It was estimated that at least ~600 collisions with Ar are required for complete relaxation.[35] This is consistent with the efficient quenching of the assigned (^{4}F) $3d^7$ tailing observed in our experiment as a result of using Ar expansion during the generation of the Fe$^+$ ions by LVI. It should be noted, however, that in the model proposed by Dougherty none of the observed mobility peaks of Fe$^+$ is assigned to a ground state.[37] In this model, the high-mobility peak (23.5 cm^2 V^{-1} s^{-1}) is assigned to the (^{2}S) $4s^13d^6$ excited state (4.56 eV above the ground state),[32] while the low-mobility peak (16.9 cm^2 V^{-1} s^{-1}) is assigned to the (^{4}D) $4s^13d^6$ second excited state (0.25 eV above the ground state).[37] These assignments cannot explain the excited-state relaxation (quenching) observed under our LVI experimental conditions, in the GD and in the EI experiments.[18,20] It is highly unlikely that potential energy curves of two states ~4.5 eV apart can cross at a distance accessible by the low collision energies used in the ion mobility experiments.

4. Nickel. The mass spectrum of the laser-generated Ni ions, displayed in Figure 5, shows the natural isotopes of Ni$^+$ with the major abundant isotope of 58 *m/z*, which is selected for the mobility measurements. The ATDs of the ^{58}Ni isotope reveal two peaks, labeled I and II in Figure 5, with a well-resolved baseline between them indicating no or negligible excited-state relaxation. The laser power study (Figure 5) indicates that the

ground state is included in peak II because the population of this peak decreases with increasing the laser power, while the excited state is included in peak I. Peak II is assigned to the (^{2}D) $3d^9$ ground state, while peak I may include the (^{4}F) $4s^13d^8$ excited state (1.160 eV) mixed with the (^{2}F) $4s^13d^8$ (1.757 eV) and the (^{4}P) $4s^13d^8$ (2.899 eV) excited states.[32] The matching between the measured ATDs and predictions from transport theory is very good. The zero-field reduced mobilities for the Ni ion electronic states are measured as 16.3 and 24.1 cm^2 V^{-1} s^{-1} for the ground and excited states, respectively. These values match nicely with those reported from the EI and GD sources.[18,20] However, the population of the excited state observed in the LVI experiments does not exceed 30% at the highest laser power used, which is much lower than that produced by the 30 eV EI of Ni(CO)$_4$ as shown in Table 1.[20]

5. Copper. The ATDs of the ^{63}Cu ion indicate two well-resolved peaks labeled I and II as shown in Figure 6. The laser power study (not shown) indicates that the ground state is included in the mobility peak II while the excited state is included in the high-mobility peak I. The low-mobility peak II is assigned to the (^{1}S) $3d^{10}$ ground state, while the high-mobility peak I is assigned to the (^{3}D) $4s^13d^9$ first excited state (2.808 eV).[32] The second excited state of Cu$^+$ (^{1}D) $4s^13d^9$ should have a very similar mobility to that of the ^{3}D state. However, given that the amount of the excited state of Cu$^+$ formed under the current LVI experimental conditions is so small relative to the ground state as shown in Figure 6, a contribution to peak I from
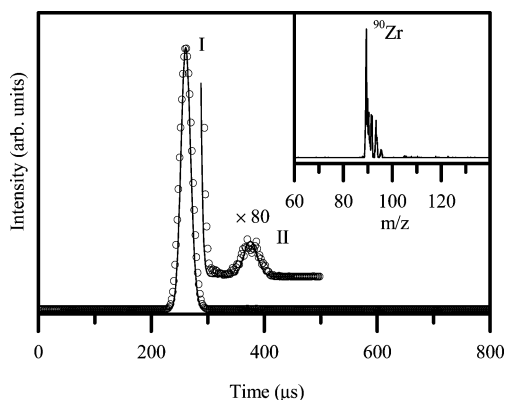
Figure 7. Experimental ATDs of Zr^+ ions (circles) and the predicted distributions from transport theory (solid line). The inset shows the mass spectrum of Zr^+ ions.

the higher-energy ^1D state (3.256 eV)[32] is unlikely. Charge-transfer bracketing experiments could provide good tests for the presence of the ^1D state. No relaxation of the excited state is observed, at least under our experimental conditions, as the matching between the measured ATDs and the predictions from transport theory is excellent and because the two peaks I and II are baseline-separated. The ground state represents the major part of the ion beam even at the highest laser power used while the excited state does not exceed 20%. The reduced mobilities for peaks I and II are measured as 24.1 and 16.1 cm^2 V^{-1} s^{-1}, respectively. The measured mobility for the ground state is in good agreement with the values obtained using EI (15.7)[18] and GD (15.8)[20] sources. However, the reduced mobility of the excited state (24.1 cm^2 V^{-1} s^{-1}) is higher than that measured using the GD source (22 ± 1 cm^2 V^{-1} s^{-1}). Kemper and Bowers[18] did not observe the excited state of Cu^+ using EI ionization of $Cu(CH_3COO)_2$ although it was observed by EI of $Cu(CH_3COO)$.[38]

6. Zirconium. The mass spectrum of the laser-generated Zr^+ (displayed in the inset of Figure 7) shows many isotopes of Zr with the highest abundant isotope at $m/z = 90$. The ATDs of ^{90}Zr ion shown in Figure 7 indicate the presence of two peaks I and II with the population of peak II less than 1% of that of peak I. The comparison of the ATDs with transport theory is very satisfactory as shown in Figure 7. The reduced mobilities measured for peaks I and II are 25.3 and 17.2 cm^2 V^{-1} s^{-1}, respectively. Because of the very low abundance of peak II, it was not possible to perform a laser power study to assign the ground and excited states. However, the assignment of ATD peaks of Zr ions can be tentatively made based on electronic states of Ti^+ observed in the EI source.[18] On the basis of the Ti^+ assignments made by Kemper and Bowers and the electronic states available to Zr^+ (Table 3), peak I can be assigned to the (^4F) $5s^14d^2$ ground state probably mixed with the (^2D), (^2P), (^2F), and (^4P) $5s^14d^2$ excited states because they all have the same electronic configuration. Peak II can be assigned to the (^2G) $4d^3$ and (^2H) $4d^3$ excited states, which have stronger attractive potential with He than the states of the $5s^14d^2$ configuration. The fact that peaks I and II are well-resolved indicates that there is no excited-state relaxation occurring as a result of the collisions with He. This may suggest that collisonal deactivation of the low-mobility excited states requires collisions with energies higher than the available collision energies in the drift cell.

7. Niobium. Niobium has only one isotope at $m/z = 93$ as shown in the inset of Figure 8. The ATDs of Nb^+ indicate two peaks that exhibit weak laser power dependence as shown in
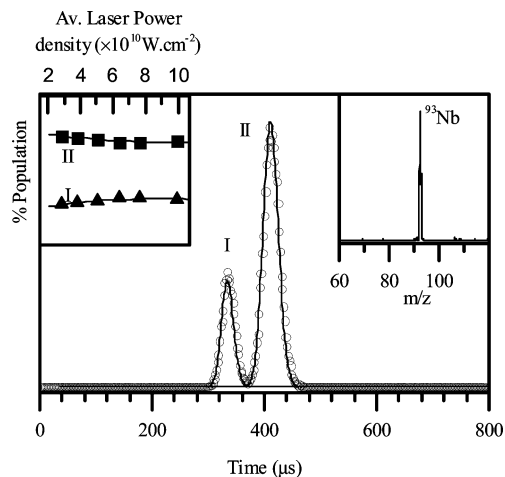

Figure 8. Experimental ATDs of Nb^+ ions (circles) and the predicted distributions from transport theory (solid line). The insets show the mass spectrum of Nb^+ ions (right) and the effect of laser power on the populations of the Nb^+ ion ground state II (squares) and excited state I (triangles).
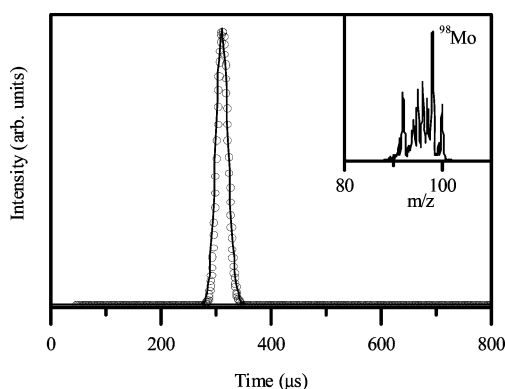

Figure 9. Experimental ATDs of Mo^+ ions (circles) and the predicted distributions from transport theory (solid line). The inset shows the mass spectrum of Mo^+ ions.

Figure 8. The laser power study indicates that the ground state ($4d^n$ configuration) is tentatively included in the lower-mobility peak II while the excited state ($5s^14d^{n-1}$ configuration) is included in peak I. The (^5D) $4d^4$ ground state in peak II is probably mixed with the (^3P) $4d$,[4] (^3H) $4d^4$, and (^3G) $4d^4$ excited states. This mixing may explain the weak laser dependence observed. Because the excitation energies of the $5s^14d^3$ states are low and the transitions to the ground state are spin-forbidden, the existence of more than one excited state under peak I is also possible. Therefore, peak I could be assigned to a mixture of the (^3F) $5s^14d^3$ and (^5P) $5s^14d^3$ excited states (Table 3). The excellent matching between the measured ATDs and the predictions from transport theory for two independent species indicates negligible relaxation of excited states inside the drift cell. Because no deactivation appears to be occurring with He, the presence of low-mobility excited states could be negligible. This would suggest that peaks II and I in Figure 8 are due to the ground and first excited states of Nb^+, respectively. The reduced mobilities of peaks I and II are measured as 19.7 and 15.5 cm^2 V^{-1} s^{-1}, respectively.

8. Molybdenum. Molybdenum has many naturally abundant isotopes as shown in the inset in Figure 9. Figure 9 indicates the presence of one peak in the ATD of Mo^+. Variation of the laser power over a wide range did not show the appearance of a second mobility peak. This suggests that the observed peak in the ATD of Mo^+ can be assigned to the ground state. The

Ion Mobility of Laser-Generated Cations

J. Phys. Chem. A, Vol. 112, No. 6, 2008 **1119**

reduced mobility of this peak is calculated as 20.6 cm^2 V^{-1} s^{-1}, indicating a high-mobility electronic state. However, this assignment is inconclusive and may require further investigation and analysis as discussed below.

The low-lying electronic states of Mo$^+$ (Table 3) indicate that the (^{6}S) ground state has the 4d^5 configuration. The first excited state is (^{6}D) 5s^{1}4d^4 and has a parity forbidden transition to the ground state. The higher excited states with the 4d^5 configuration have spin and parity forbidden transitions to the ground state and therefore are expected to have metastable lifetimes and show the same mobility as the ground state. However, because the first excited state (5s^{1}4d,^{4} 1.587 eV) and the next three excited states (4d^5) are close in energy (1.906, 1.950, and 2.120 eV, respectively; Table 3), they are expected to collisionally deactivate into the first excited state.[18] This suggests that most of the excited-state population should be in the first excited state (5s^{1}4d^4) and not with the ground state (4d^5), and this should result in two separate mobility peaks. This is clearly different from the observed one mobility peak assigned to the 4d^5 configuration.

The reduced mobilities of the ground and excited states of Mo$^+$ can be estimated based on the following trend. The mobility of a state with the 4d^n configuration is higher than that of a state with the 3d^n configuration, while states with the 5s^{1}4d^{n-1} configuration have lower mobilities than states with the 4s^{1}3d^{n-1} configuration. Because of the measured reduced mobility of the (^{6}S) 3d^5 ground state of Cr$^+$ (18.3 cm^2 V^{-1} s^{-1}), the reduced mobility of the ground state of Mo$^+$ is expected to be >18.3 cm^2 V^{-1} s^{-1}. Furthermore, becuase the reduced mobility of the (^{4}D) 4s^{1}3d^4 excited state of Cr$^+$ is 22.8 cm^2 V^{-1} s^{-1}, then the reduced mobility of the excited state of Mo$^+$ is expected to be <22.8 cm^2 V^{-1} s^{-1}. The measured reduced mobility of Mo$^+$ (20.6 cm^2 V^{-1} s^{-1}), based on one peak in the ATD shown in Figure 9, lies between the expected values of the ground and excited states. This may suggest that the measured reduced mobility of Mo$^+$ represents an average value of both of the mobilities of the ground and excited states. In fact, the very recent measurements of the mobility of Mo$^+$ generated by EI ionization of molybdenum hexacarbonyl show two ATD peaks assigned to ground and excited states with reduced mobilities of 18.5 ± 1.9 and 23.4 ± 2.3 cm^2 V^{-1} s^{-1}, respectively.[23] Therefore, the present Mo$^+$ data are inconsistent with previous results and are unique among our data for the second-row metals. It is perhaps conceivable that the excited- and ground-state mobilities are close in value as to be unresolved, but why this should only be true for Mo$^+$ is unclear. Although the well-resolved mass spectrum of the Mo$^+$ isotopes, shown in the inset of Figure 9, eliminates the possibility of having a Mo−X$^+$ adduct (where X falls in the Mo isotope range) instead of Mo$^+$, other unknown experimental effects cannot be ruled out. It is clear that the Mo$^+$ mobility measured in the LVI experiments requires further investigation and analysis.

9. Palladium. The mass spectrum of the laser-generated Pd$^+$ (displayed in the inset of Figure 10a) shows the natural isotopes of Pd with the highest abundant isotope at $m/z = 106$. The low-lying electronic states for Pd$^+$ and Ni$^+$ are similar (Tables 2 and 3) except for the excitation energies that are higher in the case of Pd$^+$. The ATDs of Pd$^+$ are composed of two peaks labeled I and II as shown in Figure 10a. On the basis of the Ni$^+$ electronic-state assignment, peaks II and I of the Pd$^+$ can be assigned to the ground and first excited states, respectively. However, the relative population of these assigned states does not show strong dependence on the laser power. To confirm the excited state's assignment of Pd$^+$, a small amount of Ar
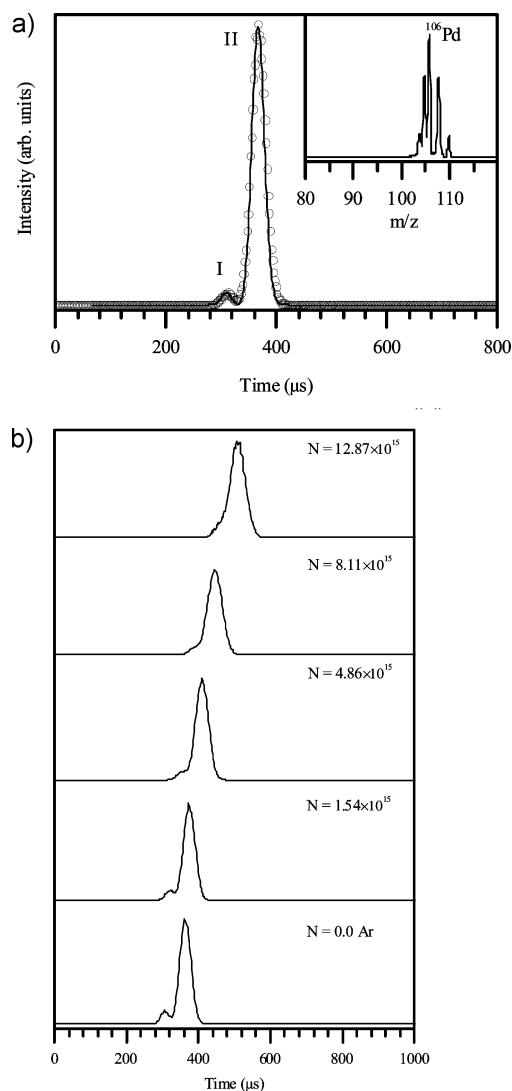

Figure 10. (a) Experimental ATDs of Pd$^+$ ions (circles) and the predicted distributions from transport theory (solid line). The inset shows the mass spectrum of Pd$^+$ ions. (b) ATDs of Pd$^+$ ions in the presence of different Ar number densities in 2.5 Torr He in the drift cell showing the deactivation of excited states by Ar.

gas with variable proportions in He is introduced into the drift cell to quench the excited states. Figure 10b shows the effect of the Ar number density inside the drift cell on the populations of the Pd$^+$ electronic states. From this data, the deactivation rate coefficient is estimated as (6−8) × 10^{-14} cm^3 s^{-1}. This is consistent with the expected greater collisional relaxation efficiency of Ar over He. It is clear from the observed quenching effect shown in Figure 10b that the Pd$^+$ excited state is included in peak I, thus confirming the assignment based on the Ni$^+$ results. The reduced mobilities of the (^{4}F) 5s^{1}4d^8 excited state (peak I) and the (^{2}D) 4d^9 ground state (Peak II) are measured as 22.9 and 18.1 cm^2 V^{-1} s^{-1}, respectively. The measured mobilities match well with those measured using the GD source as shown in Table 1.[20]

10. Silver. The mass spectrum of the laser-generated silver ions (inset of Figure 11) shows two well-resolved peaks corresponding to the natural isotopes of Ag. The ATDs of Ag$^+$ show two well-separated peaks labeled I and II as shown in Figure 11. The laser power study (inset of Figure 11) shows that the ground state (^{1}S, 4d^{10}) is included in peak II, while the excited state (^{3}D, 5s^{1}4d^9) is included in the high-mobility peak I. The comparison of the measured ATDs and the predictions
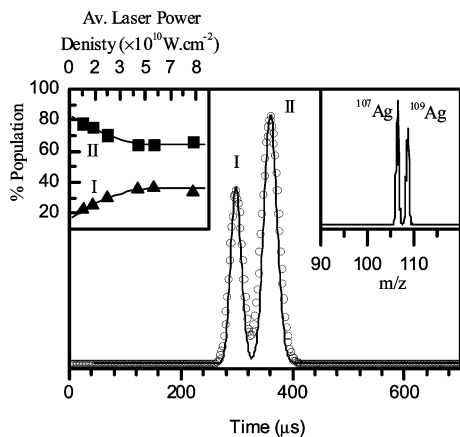
Figure 11. Experimental ATDs of Ag$^+$ ions (circles) and the predicted distributions from transport theory (solid line). The insets show the mass spectrum of Ag$^+$ ions (right) and the effect of laser power on the populations of the Ag$^+$ ion ground state II (squares) and excited state I (triangles).

of the transport theory shown in Figure 11 could suggest small relaxation of the excited state indicated by the filling between the two mobility peaks. This can be confirmed by an Ar quenching study similar to the Pd$^+$ case. A detailed quenching study using Ar and other gases is currently in progress, and the results will be published elsewhere.[34] The reduced mobilities of peaks I and II are measured as 22.1 and 17.7 cm^2 V^{-1} s^{-1}, respectively. The reduced mobility of the ground state of Ag$^+$ is higher than that of Cu$^+$, while the reduced mobility of the excited state of Ag$^+$ is lower than that of Cu$^+$. This result is consistent with the general trend observed in comparing the mobilities of the first- and second-row transition metal cations. The Ag$^+$ ground-state mobility matches well the previously measured value using the GD ion source.[20] No excited states of Ag$^+$ were observed in the GD ion source.[20] The first excited state of Ag$^+$ is 5.03 eV above the ground state, and populating such a state requires a high-energy ion source. It is clear that the LVI ion source can access this excitation energy. It is, however, intriguing that the amount of Ag$^+$ (^{3}D) (Figure 11) produced by the LVI source is much more than that of Cu$^+$ (^{3}D) (Figure 6) despite the fact that the excited-state energy of Ag$^+$ (5.034 eV) is significantly higher than that of Cu$^+$ (2.808 eV). This may suggest that the excited states of Ag$^+$ and Cu$^+$ are produced by different mechanisms during the LVI process. This point requires further investigation to evaluate the contributions of the different mechanisms responsible for ion production in the LVI process.

11. Cadmium. Figure 12 shows the mass spectrum and the ATD of the laser-generated Cd$^+$ ions. The ATD of Cd$^+$ shows only one peak under a variety of experimental conditions such as the laser power, the expansion gas, the pressure, and the applied field in the drift cell. The observed peak can be assigned to the (^{2}S) 5s^{1}4d^{10} ground state of Cd$^+$. The (^{2}P) 5p^{1}4d^{10} first excited state is 5.68 eV above the ground state, and the transition to the ground state is both parity- and spin-allowed, so it is unlikely to observe the excited state of Cd$^+$ consistent with the ATD shown in Figure 12. The high-mobility value measured for the ground state (22.2 cm^2 V^{-1} s^{-1}) is expected for a state with the 5s^{1}4d^{10} configuration due to the repulsive interaction with the filled 1s^2 orbital of He. In fact, the measured mobility of the (^{2}S) 5s^{1}4d^{10} ground state of Cd$^+$ (22.2) is similar to that of the (^{2}D) 5s^{1}4d^9 excited state of Ag$^+$ (22.1) due to the presence of the 5s electron.

12. Platinum. The mass spectrum of the laser-generated Pt$^+$ (displayed in the inset of Figure 13) shows the natural isotopes
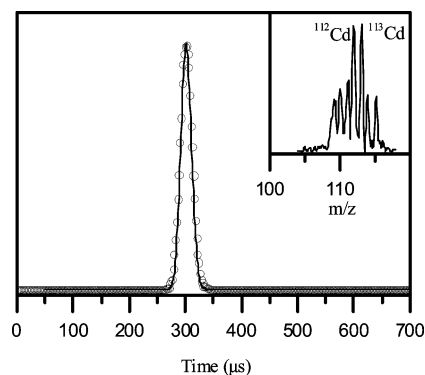

Figure 12. Experimental ATDs of Cd$^+$ ions (circles) and the predicted distributions from transport theory (solid line). The inset shows the mass spectrum of Cd$^+$ ions.
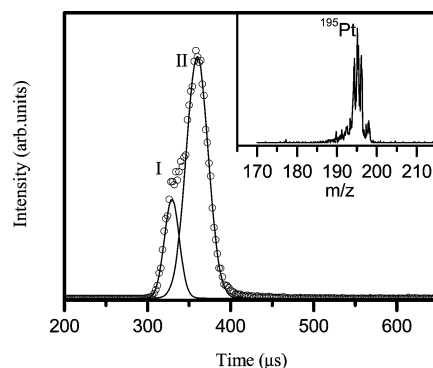

Figure 13. Experimental ATDs of Pt$^+$ ions (circles) and a Gaussian fit for two electronic states. The inset shows the isotopic distribution of Pt$^+$ ions.

of Pt with the highest abundant isotope at $m/z = 195$. The ATDs of Pt$^+$ are composed of two unresolved peaks labeled I and II as shown in Figure 13. The ATDs can be fitted to two peaks that provide a very good description of the measured ATDs as shown in Figure 13. The low-mobility peak II is assigned to the ground state of Pt$^+$ (^{2}D, 5d^9). The high-mobility peak I is assigned to the excited states of Pt$^+$, which appear to be efficiently produced in the presence of Ar carrier gas during the LVI process. It is believed that Penning ionization (through the metastable Ar* with energy of 11.5 eV) contributes significantly to the generation of the excited states in Pt$^+$.[27] The excited states with the 6s^{1}5d^8 configuration are either ^{2}F, ^{2}P, or ^{2}F with excitation energies of 1.177, 2.366, and 2.529 eV, respectively (Table 3). The production of excited states of Pt$^+$ via collisions of Ar* (11.5 eV) with Pt atoms is energetically possible because IP(Pt) + [E(^{2}F) − E(^{2}D)] = 11.1 eV < 11.5 eV.[32] This point will be further discussed in the following section dealing with the effect of the expansion carrier gas on the production of excited states.

The reduced mobilities of the ground state (peak II) and the excited states (peak I) of Pt$^+$ are measured as 18.3 and 20.8 cm^2 V^{-1} s^{-1}, respectively. These values are a little lower than the measured values of 20.2 and 23 cm^2 V^{-1} s^{-1} for the Pt$^+$ ground and excited states, respectively, using the GD source.[21] Our values for the ground-state mobilities of Pt$^+$ (5d^9 configuration) and Pd$^+$ (4d^9 configuration) are similar (18.3 and 18.1 cm^2 V^{-1} s^{-1}, respectively). However, excited-state mobility (20.8 cm^2 V^{-1} s^{-1}) of Pt$^+$ (6s^{1}5d^8 configuration) is lower than that (22.9 cm^2 V^{-1} s^{-1}) of Pd$^+$ (5s^{1}4d^8 configuration). This seems to indicate that states with the 6s^{1}5d^{n-1} configuration have lower reduced mobilities than states with the 5s^{1}4d^{n-1}

Ion Mobility of Laser-Generated Cations

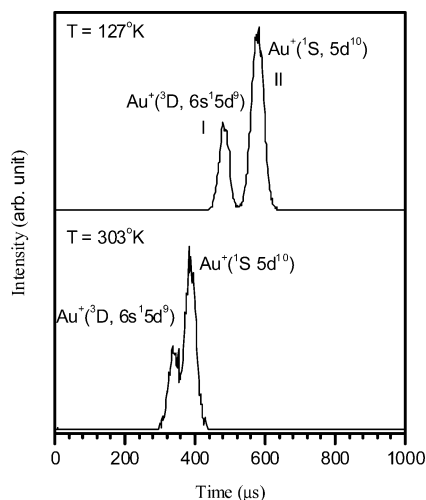*J. Phys. Chem. A, Vol. 112, No. 6, 2008* **1121**

Figure 14. Experimental ATDs of Au$^+$ ions obtained at 127 and 303 K. Note the increase in resolution with reducing the cell temperature.

configuration. This could be attributed to the larger size of the 6s-containing ions relative to the 5s-containing ions.

13. Gold. The ATDs of the Au$^+$ m/z 197 measured at two different temperatures clearly indicate the presence of two peaks I and II as shown in Figure 14. It is also clear that by lowering the temperature of the drift cell to 127 K excellent separation between the two peaks is obtained as a result of increasing the resolution of the ATDs. The low- and high-mobility peaks II and I are assigned to the ground (^1S, $5d^{10}$) and excited (^3D, $6s^15d^9$) states of Au$^+$, respectively. The reduced mobilities of the ground and excited states are measured as 18.1 and 20.4 cm^2 V^{-1} s^{-1}, respectively. The measured reduced mobility of the Au$^+$ ground and excited states produced in the GD ion source (19.5 $\pm$ 0.5 and 22.5 $\pm$ 2 cm^2 V^{-1} s^{-1}, respectively) are a little higher than the corresponding values measured in the current LVI experiments.

14. Observed Trends and Comparison with Other Ion Sources. The above results involving first-, second-, and third-row transition metal cations generated by the LVI process allow the extraction of some useful trends and the comparison with other ion sources such as the EI and GD sources. The EI study of Kemper and Bowers of the first-row transition metal ions established a general trend that ions with electronic states of the $3d^n$ configuration have low mobility while those with $4s^13d^{n-1}$ configurations have higher mobilities.[18] For this reason, the ground states of Mn$^+$, Fe$^+$, and Zn$^+$ exhibit high mobilities and therefore appear at shorter times in He relative to the corresponding electronically excited ions. However, the ground-state ions of Ti$^+$, V$^+$, Cr$^+$, Co$^+$, Ni$^+$, and Cu$^+$ have low mobilities and appear at longer times in He relative to the corresponding excited ions. As shown in Table 1, the LVI results of V$^+$, Cr$^+$, Fe$^+$, Ni$^+$, and Cu$^+$ are consistent with this trend.

On the basis of the measured mobilities of the laser-generated atomic metal cations studied here, a general trend appears to emerge. The reduced mobility of a state with the $4d^n$ configuration is higher than that of a state with the $3d^n$ configuration, while states with the $5s^14d^{n-1}$ configuration have lower reduced mobility than states with the $4s^13d^{n-1}$ configuration. Our results of Zr$^+$, Nb$^+$, Pd$^+$, Ag$^+$, Cd$^+$, Pt$^+$, and Au$^+$ confirm that the first-row trend established by Kemper and Bowers[18] is also observed for the second- and third-row transition metal ions. For example, the ground-state Zr$^+$ ions with the $5s^14d^2$ electronic configuration exhibit a high mobility of 25.3 cm^2 V^{-1} s^{-1}. The LVI results in Table 1 also indicate that the ratio between the reduced mobilities of excited and ground states decreases as

one goes from the first- to the second- to the third-row transition metal cations. For example, the ratios of the excited-state (s^1d^{n-1} electronic configuration) to the ground-state (d^n configuration) reduced mobilities for each of Ni$^+$, Pd$^+$, and Pt$^+$ are 1.48, 1.27 and 1.14, respectively. Similarly, these ratios for Cu$^+$, Ag$^+$, and Au$^+$ are 1.50, 1.25, and 1.13 cm^2 V^{-1} s^{-1}, respectively. One possible explanation of this trend is that ion size increases in the order 6s > 5s > 4s. It is also possible that higher-order attractive interactions between the metal cations and the helium increase in the order $6s^1d^{n-1}$ > $5s^1d^{n-1}$ > $4s^1d^{n-1}$. However, it should be noted that the apparent trend is less pronounced in comparing V$^+$ and Nb$^+$ where the ratios of the excited- to ground-state mobilities are 1.33 and 1.27, respectively.

The comparison between the observed mobility peaks from different ion sources reveals that the GD source generally produces fewer excited states, particularly the ones that require high excitation energies. For example, in the case of V$^+$ both the EI[18] and LVI sources show three mobility peaks corresponding to high-energy states (>2.4 eV) of the $4sd^3$ configuration, the first excited state (^5F, $4s^1d^3$, and ^3F, $4s^1d^3$) and a ground state (^5D, $3d^4$). However, the high-mobility (25 cm^2 V^{-1} s^{-1}), high-energy excited states (peak I) could not be observed in the GD source.[20] Another difference is the observation of both ground- and excited-state ions for Ag$^+$ from the LVI source while only ground states are observed in the GD source. This could be due to the higher excitation energies of Ag$^+$ (>5 eV), which may not be available in the GD source.[20] A more likely reason for the inefficient production of excited states in the GD source is the collisional deactivation of many excited states due to the high pressure typical in GD sources.[20]

The final important comparison between the LVI and the EI sources is focused on the relative populations of the excited- and ground-state metal ions. As shown in Table 1, the populations of the excited states are much lower in the LVI source as compared to the low-energy EI sources. For example, the fraction of the ground-state population measured at 17 eV ionizing energy (the AP of Ni$^+$ from Ni(CO)$_4$ = 14.75 eV) is only 60%,[18] while in the LVI experiments with a laser power of 1.5 $\times$ 10^{10} W/cm^2 at least 87% ground-state Ni$^+$ can be produced. One possible reason for this difference is that in LVI at low laser fluences the metal ions are likely to be produced by multiphoton ionization because the temperature of the plume is insufficient to generate a significant number of ions by a thermal mechanism. However, at higher fluences in the range of about 10^{12} W/cm^2 thermal and plasma processes dominate, and the vapor cloud heating could reach 10^5 K (about 13 eV) at about 6 ns while the metal surface remains near 6000 K.[1−3] At both low and high laser fluences, the excited-state ions are generated through the electronic excitations of the ground-state ions. In contrast, in the EI ionization of volatile organometallic compounds, the dissociated metal atoms and ions are already in excited states, and the populations of the ground states require efficient deactivations that may not be available under the typical vacuum conditions.

B. Effect of Experimental Parameters. In this section, we discuss the effects of the important experimental parameters of the LVI ion mobility technique on the production and population of electronically excited metal ions.

In the LVI experiments, a pulse of carrier (expansion) gas, usually Ar or He, is applied with a synchronized delay time with respect to the laser vaporization pulse. The carrier gas interacts with the laser plume and sweeps the ions toward the mass spectrometer. We recently provided evidence for the role of Penning ionization in the production of electronically excited-
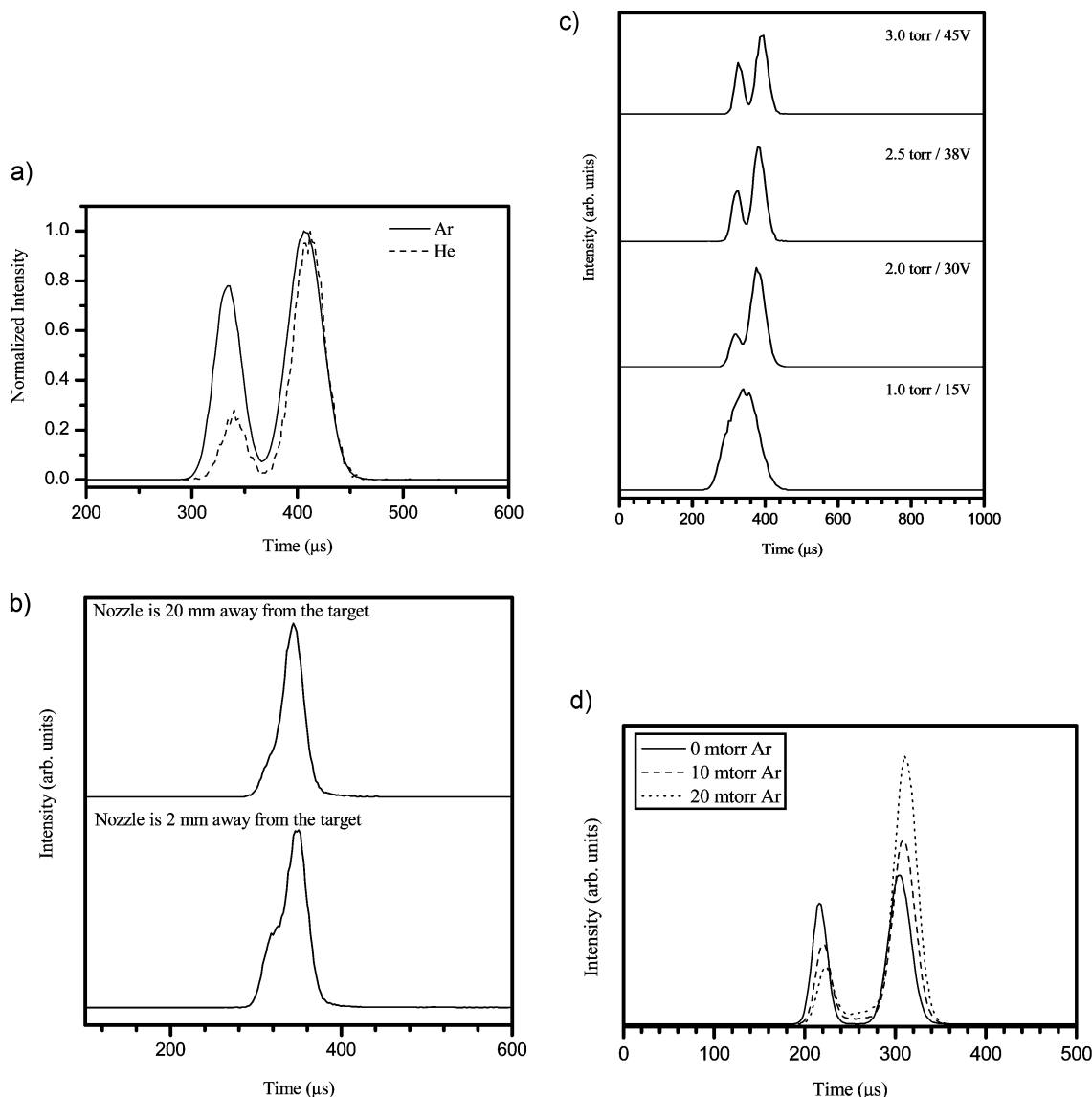
Figure 15. (a) Effect of expansion carrier gas on the population of Nb^+ electronic states. The experimental conditions (He buffer gas pressure = 2.5 Torr and $T = 300$ K) are the same for both Ar and He expansions. (b) Effect of ion source geometry on the population of Pt^+ electronic states. (c) Effect of He buffer gas pressure and drift field on resolving the Pd^+ electronic states. The arrival time distributions are collected at the same E/N value of 5.20 TD. (d) ATDs of Ni^+ electronic states collected at 2.0 Torr pure He (solid line), 2.0 Torr He + 10 mTorr Ar (dashed line), and 2.0 Torr He + 20 mTorr Ar (dotted line).

state metal ions during the laser plume in the presence of argon carrier gas.[27] The Penning ionization proceeds via Ar metastable atoms, which are known to occur at 11.5 and 11.7 eV.[32,40] The metastable Ar* atoms are favorably produced as compared to other carrier gas atoms such as He due to the higher probability of producing Ar* (11.5 eV) versus He* (19.7 eV)[32] and also the significantly higher cross-section for Penning ionization by Ar*.[40] These metastable Ar* atoms could be produced in the laser plume and also via collisions of Ar atoms with the fast electrons produced by the laser plasma vaporization. It is conceivable that Penning ionization by Ar* can enhance the production of both ground- and excited-state ions. However, by comparing the relative populations of ground- and excited-state ions produced by LVI in the presence of Ar and He, the contributions of Penning ionization were found to be significant in the production of excited states of the Ni^+, Nb^+, and Pt^+ ions.[27] For example, the collisions of metastable Ar* with the Ni atoms produced by laser vaporization would then generate the excited states of Ni^+ because the ionization potential of Ni (IP = 7.60 eV) plus the excitation energy $(E(^4P) - E(^2D) =$

$2.899 - 0.075 = 2.82$ eV) is 10.4 eV < 11.5 eV.[32] The same effect is also observed in the production of excited states from Nb^+ as shown in Figure 15a where the population of Nb^+ excited states is significantly enhanced in the Ar expansion as compared to He. The Ar* Penning ionization of Pt is also energetically possible as evident from the ATDs of Pt^+ produced by LVI in Ar expansion shown in Figure 15a.

Another important parameter that influences the production of excited states in the LVI process is the geometry of the ion source. Figure 15b compares the ATDs of Pt^+ produced by LVI using Ar as a carrier gas in two different geometries where the Pt rod is placed 20 mm and 2 mm from the supersonic nozzle orifice where the Ar expansion occurs. By placing the Pt rod very close to the nozzle, the Ar expansion pulse overlaps efficiently with the laser plume where the density of the fast electrons is high. This, in turn, increases the number density of the metastable Ar* atoms, which results in more excited states of Pt^+ as shown in Figure 15b.

The resolution of the ATD depends on the drift voltage and the temperature of the buffer gas in the drift cell (resolution is

Ion Mobility of Laser-Generated Cations

J. Phys. Chem. A, Vol. 112, No. 6, 2008 **1123**

given by $(qV/8k_BT)^{1/2}$, where q is the charge on the ion.[18] The effect of temperature is illustrated in Figure 14 where excellent separation of the excited- and ground-state mobilities of Au^+ is demonstrated at 127 K. The drift voltage also has a significant effect on the resolution of the ground- and excited-state mobility peaks. This effect is demonstrated in Figure 15c where the resolution of the ATDs of Pd^+ is dramatically improved by increasing the drift voltage. To avoid the high-field regime where the mobility is strongly dependent on the ion energy, the cell pressure must be increased proportionally to the drift voltage as illustrated in Figure 15c.

The populations of excited-state ATD peaks are also very sensitive to the presence of quenching gases such as Ar (or small impurity water vapor) in the helium buffer gas in the drift cell. Figure 15d illustrates the deactivation effect of small concentrations of Ar on the excited states of Ni^+. The observed filling between the excited- and the ground-state mobility peaks as the Ar concentration increases provides direct evidence for the deactivation between the excited and the ground states of Ni^+.

An interesting observation, which needs to be quantified, is that the excited-state populations depend on the surface properties of the vaporizing metal rod. For example, populations of the excited states are always high when using fresh metal rods where the surface oxide layers are still present. However, the excited-state populations decease gradually until the complete removal of the oxide layers (after several laser shots) after which the excited-state populations do not change in time. It appears that the metal ions produced by LVI of the oxide surface layers of the metal targets contain large populations of excited states. However, once the oxide layers are removed, the population of the excited states reaches a lower value and does not show further decrease in time. It is reasonable to assume that decomposition of metal oxides in the laser plume can result in more excited-state ions. Clearly, this effect needs further studies to understand the mechanism by which the excited states are produced from the LVI of the metal oxide surface layers.

IV. Conclusions

We presented the application of the ion mobility technique to separate the electronic states of first-, second-, and third-row transition metal cations generated by the laser vaporization/ionization (LVI) technique. LVI is a universal source for the generation of any metal cation in the gas phase, and the nature and populations of the excited states produced depend on many factors. Among these factors are the laser power, the geometry of the ion source, the nature and pressure of the carrier gas, and the presence of impurity-quenching gases. In this work we have shown that LVI using the second harmonic of the Nd: YAG nanosecond laser can access excited states with energies as high as 5 eV (Ag^+ excited state). However, in comparison with electron impact of volatile organometallic compounds, the LVI populates fewer excited states due to the combination of multiphoton, thermal, and plasma processes where the metal atoms and ions are pumped from ground- to excited-state ions. Significant contributions to the production and populations of excited states of Ni^+, Nb^+, and Pt^+ cations have been observed in the presence of argon carrier gas and attributed to the Penning ionization mechanism.

The mobility measurements for most of the laser-generated transition metal cations reveal the presence of two or three mobility peaks that correspond to ground and excited states of different electronic configurations. The similarity of the measured reduced mobilities for the metal cations generated by LVI, electron impact, and glow discharge ion sources indicates that the same electronic configurations are produced regardless of the ion source. The ratio of the reduced mobilities of the excited to the ground states decreases as one goes from the first- to the second- to the third-row transition metal cations. This trend is attributed to the increase in the ion size. In addition, higher-order attractive interactions between the metal ions and helium are expected to increase in the order $6s^1d^{n-1} > 5s^1d^{n-1} > 4s^1d^{n-1}$.

This work aimed to help understanding of the mechanisms by which transition metal cations react in the gas phase by identifying the ground and excited states that can be responsible for their reactivity. It will be beneficial if the ion mobility system is combined with another technique that characterizes the separated electronic states based on their reactivity, so electronic-state-selected chemical reactions can be studied in depth.

References and Notes

(1) Anisimov, S. I.; Luk'yanchuk, B. S. *Phys.-Usp.* **2002**, *45*, 293–324.

(2) Dreyfus, R. W. In *Laser Ablation of Electronic Materials: Basic Mechanisms and Applications*; Fogarassy, E., Ed.; Elsevier Publishers: London, 1992.

(3) *Laser Ablation: Mechanisms and Applications*; Miller, J. C., Haglund, R. F., Jr., Eds.; Lecture Notes in Physics 389; Springer-Verlag: Berlin, 1991.

(4) Kang, H.; Beauchamp, J. L. *J. Phys. Chem.* **1985**, *89*, 3364–3367.

(5) Blomberg, M.; Yi, S. S.; Noll, R. J.; Weisshaar, J. C. *J. Phys. Chem. A* **1999**, *103*, 7254–7267.

(6) Jones, R. W.; Staley, R. H. *J. Am. Chem. Soc.* **1980**, *102*, 3794.

(7) Tonkyn, R.; Weisshaar, J. C. *J. Am. Chem. Soc.* **1986**, *108*, 7128.

(8) Buckner, S. W.; Freiser, B. S. *J. Am. Chem. Soc.* **1987**, *109*, 1247.

(9) Armentrout, P. B.; Beauchamp, J. L. *Acc. Chem. Res.* **1989**, *22*, 315.

(10) Bowers, M. T. *Acc. Chem. Res.* **1994**, *27*, 324.

(11) Duncan, M. A. *Annu. Rev. Phys. Chem.* **1997**, *48*, 69.

(12) Jarrold, M. F. *Acc. Chem. Res.* **1999**, *32*, 360.

(13) Duncan, M. A. *Int. Rev. Phys. Chem.* **2003**, *22*, 407.

(14) Armentrout, P. B. Transition Metal Ion Chemistry. In *The Encyclopedia of Mass Spectrometry: Theory and Ion Chemistry*; Armentrout, P. B., Ed.; Elsevier: Amsterdam, 2003; Vol. 1, pp 800–810.

(15) Elkind, J. L.; Armentrout, P. B. *J. Phys. Chem.* **1985**, *89*, 5626.

(16) Weisshaar, J. C. Control of transition-metal cation reactivity by electronic state selection. In *State-Selected and State-to-State Ion–Molecule Reaction Dynamics*; Ng, C.-Y., Baer, M., Eds.; Advances in Chemical Physics 82; Wiley: New York, 1992; p 213.

(17) Kemper, P. R.; Bowers, M. T. *J. Am. Chem. Soc.* **1990**, *112*, 3231.

(18) Kemper, P. R.; Bowers, M. T. *J. Phys. Chem.* **1991**, *95*, 5134.

(19) Bowers, M. T.; Kemper, P. R.; von Helden, G.; van Koppen, P. A. M. *Science* **1993**, *260*, 1446.

(20) Taylor, W. S.; Spicer, E. M.; Barnas, D. F. *J. Phys. Chem. A* **1999**, *103*, 643.

(21) Taylor, W. S.; May, J. C.; Lasater, A. S. *J. Phys. Chem. A* **2003**, *107*, 2209.

(22) Taylor, W. S.; Matthews, C. C.; Parkhill, K. S. *J. Phys. Chem. A* **2005**, *109*, 356.

(23) Iceman, C.; Rue, C.; Moision, R. M.; Chatterjee, B. K.; Armentrout, P. B. *J. Am. Soc. Mass Spectrom.* **2007**, *18*, 1196.

(24) van Koppen, P. A. M.; Kemper, P. R.; Bowers, M. T. *J. Am. Chem. Soc.* **1992**, *114*, 10941.

(25) van Koppen, P. A. M.; Kemper, P. R.; Bowers, M. T. *J. Am. Chem. Soc.* **1992**, *114*, 1083.

(26) van Koppen, P. A. M.; Kemper, P. R.; Bowers, M. T. *J. Am. Chem. Soc.* **1993**, *115*, 5616.

(27) Ibrahim, Y. M.; Alsharaeh, E. H.; El-Shall, M. S. *J. Phys. Chem. B* **2004**, *108*, 3959.

(28) Rusyniak, M.; Ibrahim, Y. M.; Alsharaeh, E.; Meot-Ner, M.; El-Shall, M. S. *J. Phys. Chem. A* **2003**, *107*, 7656.

(29) Rusyniak, M. J.; Ibrahim, Y. M.; Wright, D. L.; Khanna, S. N.; El-Shall, M. S. *J. Am. Chem. Soc.* **2003**, *125*, 12001.

(30) Mason, E. A.; McDaniel, E. W. *Transport Properties of Ions in Gases*; John Wiley & Sons: New York, 1988.

(31) Kemper, P. R.; Bowers, M. T. *J. Am. Soc. Mass Spectrom* **1990**, *1*, 197.

Ibrahim et al.

(32) (a) Moore, C. E. *Atomic Energy Levels*; National Standards Reference Data Series, National. Bureau of Standards: Washington, DC, 1971; p 35. (b) *NIST Chemistry WebBook*; Linstrom P. J., Mallard, W. G., Eds.; NIST Standard Reference Database 69; National Institute of Standards and Technology: Gaithersburg MD, 2003. http://webbook.nist.gov.

(33) Aristov, N.; Armentrout, P. B. *J. Phys. Chem.* **1987**, *91*, 6178.

(34) Momoh, P.; Xie, E.; El-Shall, M. S., to be submitted for publication.

(35) Loh, S. K.; Fisher, E. R.; Lian, L.; Schultz, R. H.; Armentrout, P. B. *J. Phys. Chem.* **1989**, *93*, 3159.

(36) Partridge, H.; Bauschlicher, C. W., Jr. *J. Phys. Chem.* **1994**, *98*, 2301.

(37) Dougherty, R. C. *Mass Spectrom. Rev.* **2001**, *20*, 142.

(38) Fisher, E. R.; Elkind, J. L.; Clemmer, D. E.; Georgiadis, R.; Loh, S. K.; Aristov, N.; Sunderlin, L. S.; Armentrout, P. B. *J. Chem. Phys.* **1990**, *93*, 2676.

(39) Barnes, L. A.; Rosi, M.; Bauschlicher, C. W., Jr. *J. Chem. Phys.* **1990**, *93*, 609.

(40) Siska, P. E. *Rev. Mod. Phys.* **1993**, *65*, 337.